An Experimental and Theoretical Investigation of a 2 μm Wavelength Low-Threshold Microsphere Laser

An Experimental and Theoretical Investigation of a 2 μm Wavelength Low-Threshold Microsphere Laser

Jibo Yu, Xin Wang, Wenhao Li, Meng Zhang, Jiquan Zhang, Ke Tian, Yanqiu Du, Síle Nic Chormaic, and Pengfei Wang

***Abstract*—We present our results on an experimental and theoretical investigation into a glass microsphere laser emitting at 2 μm wavelength. First, we fabricated Ho^{3+}-doped tellurite glass fiber and measured the absorption and emission spectra, and the fluorescence lifetime. Using this fiber, a tellurite glass microsphere with a Q-factor of 2×10^6 was also prepared, and a single-mode laser output with a low threshold of 342 μW was observed using a 1150 nm laser as the pump source. The dynamic characteristics of the microsphere laser were studied theoretically by considering rare-earth ion spectroscopy, the rate equation of the rare-earth energy level, and the light-matter interactions in the microsphere. This work can be used to study laser emissions with low thresholds in rare-earth doped compound glass microresonators for a wide range of applications, such as gas sensing, integrated photonics, and medical surgery.**

***Index Terms*—Microcavity, microsphere laser, tellurite glass.**

I. Introduction

In THE past few decades, the level of research activity surrounding spherical geometry, microcavity resonators has increased rapidly [1], [2]. Normally, pump light from an external source is coupled into the microcavity through a prism or a tapered fiber via the evanescent wave interaction. The mode which supports light propagation near the surface of the sphere is referred to as a whispering galley mode (WGM). The small size and the high uniformity of the microcavity combine to yield an extremely high quality (Q) factor and small mode volume. Whispering gallery microresonators have many important applications, such as active and passive photonics devices, optical feedback, nonlinear optics, low laser threshold devices, opto-mechanics, non-reciprocity photonic devices, dispersion managed optical systems, and energy storage [3]–[11].

The high-Q and small mode volume of the microcavity facilitate the realization of highly efficient, light-matter interactions, with many studies on microcavity lasers and active amplifiers having been reported [12]–[18]. It should be noted that, to date, the material of choice for microcavities has been predominantly silica, which is limited by the rare-earth doping concentration and the low transmittance for use in the mid-infrared wavelength band. These drawbacks can be effectively overcome by using compound glasses or glass ceramics [19] as the host material, as they exhibit a low phonon energy, a high doping concentration, and high optical transmittance. A number of studies have focused on compound glass microcavity lasers and optical amplifiers [20]–[27] and several theoretical works have aimed at optimizing the microcavity design [28]–[30]. However, the influence of the host materials have often been overlooked in earlier experimental and theoretical investigations into microsphere lasers, including the significant aspects of characterization of the doped compound glass, Judd-Ofelt (J-O) theoretical analysis, and the study of the rate equations in rare-earth ion [31]–[33].

In this paper, we investigate, both experimentally and theoretically, a microsphere laser based on Ho^{3+} doped tellurite glass with emissions around 2 μm. In the experiment, Ho^{3+} doped bulk glass was characterized and the threshold curve of a microsphere laser was measured. The relevant parameters of the material, such as the absorption and emission cross-sections, fluorescence branch ratio, lifetime, etc., were obtained based on a J-O theoretical analysis. Next, a mathematical model was developed for the entire microsphere system which included the doped compound glass material. Finally, we calculated the dynamic processes of the output laser using dedicated in-house developed software.

The paper is divided into four parts: (i) a description of the preparation of the Ho^{3+} doped tellurite glass and fiber, (ii)

Manuscript received September 20, 2019; revised October 28, 2019; accepted December 3, 2019. Date of publication December 9, 2019; date of current version April 1, 2020. The work was supported in part by the National Key R&D Program of China under Grant 2016YFE0126500, in part by the National Natural Science Foundation of China under Grant 61575050 and Grant 61805074, in part by the Fundamental Research Funds for the Central Universities under Grant HEUCFG201841, in part by the Key Program for Natural Science Foundation of Heilongjiang Province of China under Grant ZD2016012, in part by the Open Fund of the State Key Laboratory on Integrated Optoelectronics under Grant IOSKL2016KF03, and in part by the 111 Project (B13015) to the Harbin Engineering University. The work of S. N. C. was supported by the OIST Graduate University. *(Corresponding author: Pengfei Wang.)*

J. Yu, X. Wang, W. Li, M. Zhang, J. Zhang, and K. Tian are with the Key Laboratory of In-fiber Integrated Optics of Ministry of Education College of Science-Harbin Engineering University, Harbin 150001, China (e-mail: yu20131164@hrbeu.edu.cn; wangxinok@hrbeu.edu.cn; lwh19950225@163.com; meng zhang@hrbeu.edu.cn; 1037706223@qq.com; ketian@hrbeu.edu.cn).

Y. Du is with the Key Laboratory of In-Fiber Integrated Optics of Ministry of Education, College of Science Harbin Engineering University, Harbin 150001, China, and also with the School of Electronics and Information Engineering, Heilongjiang University of Science and Technology, Harbin 150022, China (e-mail: hellen_q@126.com).

S. Nic Chormaic is with the Light-Matter Interactions for Quantum Technologies Unit, Okinawa Institute of Science and Technology Graduate University, Onna 904-0495, Japan (e-mail: sile.nicchormaic@oist.jp).

P. Wang is with the Key Laboratory of In-Fiber Integrated Optics of Ministry of Education, College of Science Harbin Engineering University, Harbin 150001, China, and also with the Key Laboratory of Optoelectronic Devices and Systems of Ministry of Education and Guangdong Province College of Optoelectronic Engineering, Shenzhen University, Shenzhen 518060, China (e-mail: pengfei.wang@tudublin.ie).

Color versions of one or more of the figures in this article are available online at https://ieeexplore.ieee.org.

Digital Object Identifier 10.1109/JLT.2019.2958349

the characterization of the Ho^{3+} doped tellurite glass, (iii) the fabrication and experimental characterization of the microsphere laser, and (iv) theoretical analysis.

II. Preparation of the Ho^{3+} Doped Tellurite Glass and Fiber

Firstly, a Ho^{3+} doped tellurite glass sample with composition of $72TeO_2$-$20ZnO$-$5Na_2CO_3$-$2Y_2O_3$-$1HoF_3$ (in mol%) was fabricated by the method of melt-quenching [34]. 15 g of high-purity chemical material (TeO_2 (99.99%), ZnO_2 (99.99%), Na_2CO_3 (99.99%), Y_2O_3 (99.99%) and HoF_3 (99.99%)) was placed in an agate mortar and stirred for 10 minutes, stored in an alumina crucible, and heated in a closed furnace at 850 °C for 90 minutes. The melt was poured on a brass sheet for rapid cooling and then transferred to a precision annealing furnace at 250 °C for 3 hours to remove any remnant internal stress. The tellurite glass fiber was fabricated by inserting a quartz rod into a crucible containing the molten glass at a suitable viscosity and rapidly drawing it; it could also be prepared using a fiber drawing tower [35].

The prepared Ho^{3+} doped tellurite glass fiber was mounted on a high-precision, three-dimensional displacement platform, a weight was hung at the lower end of the fiber, and a CO_2 laser was focused on the glass fiber to obtain a tapered fiber with a waist of 20 μm diameter. Next, an appropriately high-power laser was focused on the waist of the tapered fiber to form a microsphere with a diameter of about 41.8 μm. Compared to the method of heating and forming at the tip of a tapered fiber [27], the microspheres heated in the waist region have better axial symmetry.

III. Characterization of the Ho^{3+} Doped Tellurite Glass

The prepared tellurite glass was double-side polished to a thickness of 2.25 mm, and its absorption spectrum was measured using a spectrophotometer (LAMBDA 750, PERKINELMER, USA). The energy levels of the Ho^{3+} ions are marked on the corresponding absorption peaks in Fig. 1(a). The emission spectrum of tellurite glass is shown in Fig. 1(b) and was obtained using a 1150 nm single-mode fiber laser, chopper, and spectrometer (DEC-M204, ZOLIX, China). The inset in Fig. 1(b) is an enlarged view of the band in the wavelength range 2600 to 3200 nm. Clearly, the intensity of the fluorescent emission is very weak, and it can be attributed to the large absorption at the 3 μm wavelength induced by OH- ions [36], [37], resulting in a large loss in the tellurite glass and could not be detected in the emission spectrum. To characterize the spontaneous emission of Ho^{3+} ions from a high energy level to the ground state in tellurite glass, the fluorescence lifetimes at wavelengths of 2 μm and 2.8 μm were measured, as shown in Fig. 1(c). The lifetimes of the 2 μm and 2.8 μm emission after exponential fitting are 3.4 ms and 0.4 ms, respectively.

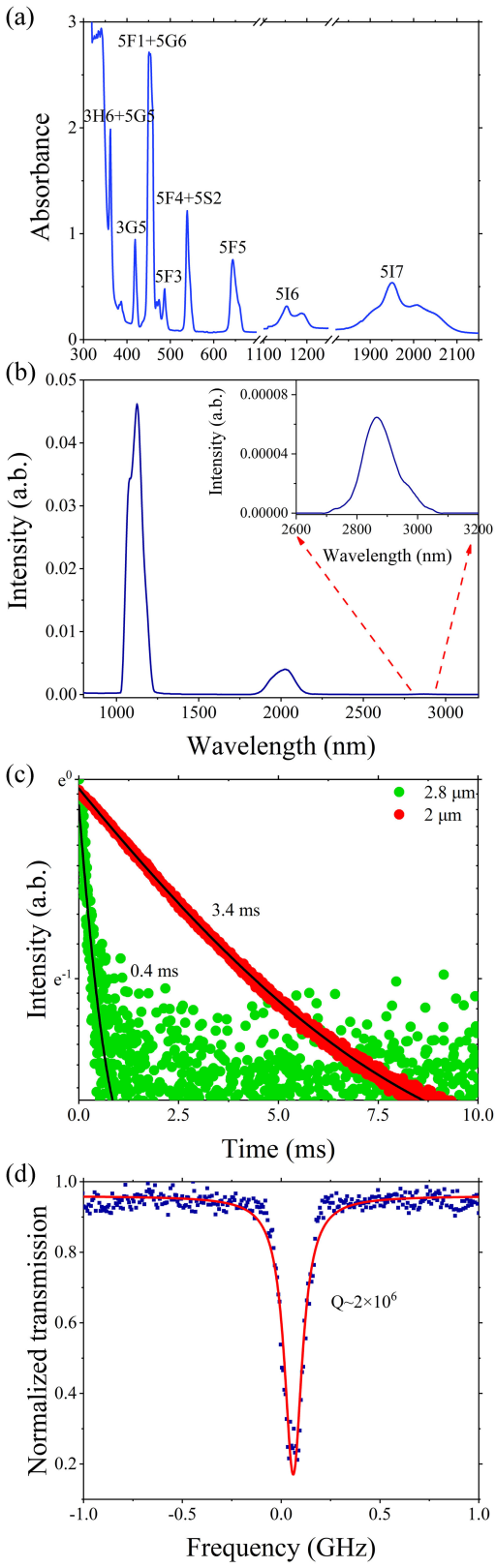

Fig. 1. (a) Absorption spectrum of the doped bulk tellurite glass. The energy levels are marked on the corresponding peaks. (b) Emission spectrum of the doped bulk tellurite glass. Inset: zoomed region from 2600–3200 nm. (c) Fluorescence lifetime measurement of the 2 μm and 2.8 μm emission. (d) The blue dots represent the normalized transmission through the coupling fiber using a 1550 nm tunable laser, and the red line represents the Lorentz fit of the blue dots. (a.b.) represents arbitrary units.

IV. Experimental Characterization of the Microsphere Laser

The Q-factor of the Ho^{3+} doped microsphere was measured by scanning the frequency of a tunable laser (TL) (TSL-710, Santec, Japan), where the center wavelength was 1550 nm. The repetition frequency of the signal generator and the scanning frequency of one period was set to 50 Hz and 15 GHz, respectively. The resulting normalized transmission curve is shown in Fig. 1(d), from which the corresponding Q-factor of the microsphere was calculated to be 2×10^6. It should be noted that the microsphere and tapered fiber are in contact in order to keep the whole system more stable and this leads to an under-coupling of the resonance [38].

A single-mode fiber laser with a wavelength of 1150 nm was chosen as the pump light source for the Ho^{3+} doped tellurite microsphere. The diameters of the tapered fiber and the microsphere were 2 μm and 41.8 μm, respectively, as described in the previous section. A microscope image of the microsphere is shown in Fig. 2(a). When the pump power rose above the threshold of 324 μW, single-mode lasing was observed using an optical spectrum analyzer (OSA) (AQ6375B, Yokogawa, Japan), see Fig. 2(b). A free spectral range (FSR) of 17.7 nm was observed from the fluorescence emission peak and this agrees well with the theoretical calculation result of 17.8 nm [39]. The OSA has a spectral resolution of 0.02 nm, making it impossible to experimentally measure the linewidth of the output laser. The fluorescence emission spectrum of Ho^{3+} doped tellurite glass is also shown in Fig. 2(b) for comparison.

Figure 2(c) shows the relationship between the measured single-mode laser output and the pump power. It is worth noting that, when the pump power is lower than the threshold, the emission process in the microsphere is governed only by fluorescence from the Ho^{3+} ions. In this region, the linearity of the fitted line is excellent. However, for pump power values higher than 342 μW (the threshold value), the linearity of the fitted line is not perfect (variance $s^2 = 0.955$). The departure from linearity can be attributed to a high refractive index difference between the silica tapered fiber and the tellurite microsphere, and mode competition is more likely to occur in the gain interval. The condition for single-mode output was observed throughout the entire threshold curve measurement cycle and the resulting conversion efficiency was calculated to be 0.55% as the slope of the linear fit in this region. For comparison, Table I lists the threshold and corresponding conversion efficiencies of microsphere lasers having an output wavelength around 2 μm reported in recent years. It should be noted that all power thresholds are the absolute pump power rather than the coupled pump power.

V. Theoretical Analysis

In order to better understand the role of the host material in the behavior of the microsphere laser, we performed a theoretical analysis by using the relevant parameters obtained from the experiment. The theoretical analysis is divided into the two parts. The first deals with a solution of the theoretical emission probability and fluorescence lifetime of the $^5I_6$ and $^5I_7$ energy

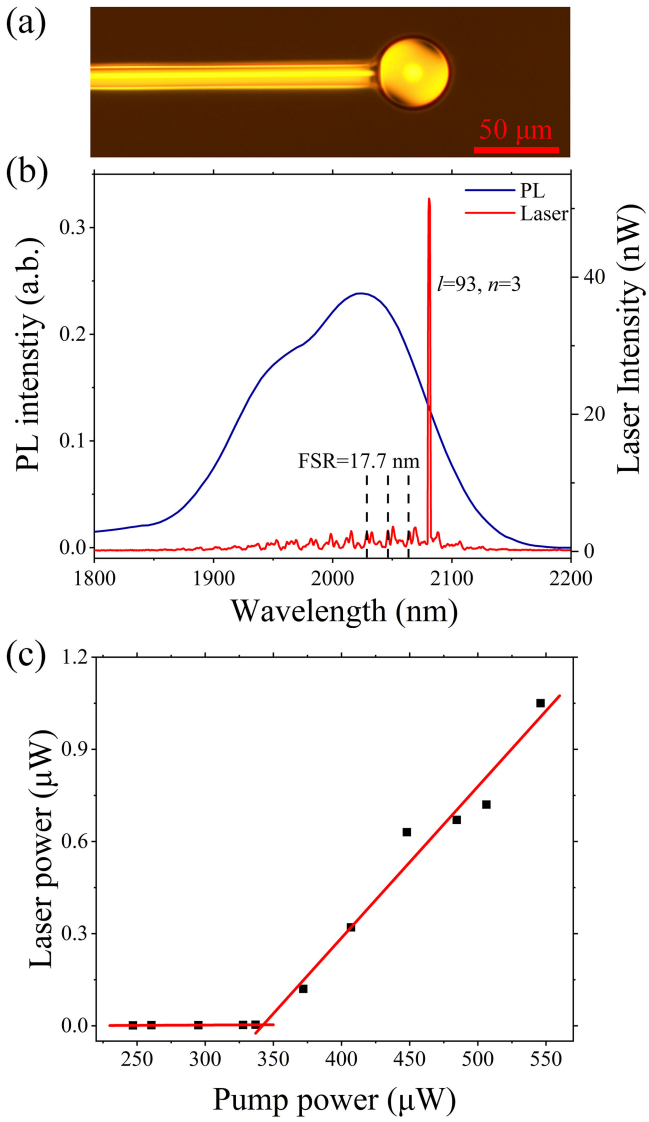

Fig. 2. (a) A microscope image of a Ho^{3+} doped tellurite microsphere. (b) The spectrum of the single-mode output laser (red line) from the microsphere and the corresponding fluorescence spectrum (blue line) from bulk glass. The dashed line indicates that the measured FSR is about 17.7 nm. (c) A fitting threshold curve for the laser output power as a function of the pump power showing a threshold of 342 μW. (a.b.) represents arbitrary units.

levels in Ho^{3+} doped tellurite glass using J-O theory [31], [46], [47]. The second is dedicated to a solution of the internal dynamic characteristic processes inside the microsphere.

The absorption peaks of the Ho^{3+} ions are shown in Fig. 1(a), from which the corresponding absorption cross-sections, σ_{abs}, were obtained. The experimental spectral line strength (S_{exp}) of the SLJ level to the S′L′J′ transition of the $4f^N$ electronic configuration in the rare-earth ion was calculated as follows [31]:

$$S_{\mathrm{exp}}(J \to J') = 0.2 \times 10^3 \times \frac{n_s \times (2J+1)}{({n_s}^2+2)^2 \times \overline{\lambda} \times N_0 \times L}$$

TABLE I
RESEARCH PROGRESS OF 2 MICRON MICROSPHERE LASER

Gain medium	Substrate materials	Wavelength	Threshold	Conversion efficiency	Reference
Tm^{3+}	Fluoride glass	1.89 μm	4.5 mW	0.0015%	[40]
Ho^{3+}-Tm^{3+}	Silica glass	1.99 μm	3.1 mW	0.022%	[41]
Tm^{3+}	Silica glass	2.04 μm	1.2 mW	0.01%	[42]
Yb^{3+}-Ho^{3+}	Silica glass	2.01 μm	14.7 mW	0.002%	[43]
Ho^{3+}-Tm^{3+}	Tellurite glass	2.09 μm	0.88 mW	0.02%	[44]
Tm^{3+}	Tellurite glass	2 μm	20 mW	0.7%	[45]
Ho^{3+}	Tellurite glass	2.08 μm	0.34 mW	0.55%	This work

TABLE II
EXPERIMENTAL AND THEORETICAL LINEWIDTH STRENGTH OF CORRESPONDING ENERGY LEVEL TRANSITION

Transition	U(2)	U(4)	U(6)	S_{exp} (cm^2)	S_{theory} (cm^2)
$^3G_5$-$^5I_8$	0.00	0.53	0.00	3.71×10^{-20}	4.70×10^{-20}
$^5G_6$-$^5I_8$	1.52	0.84	0.14	1.28×10^{-19}	1.28×10^{-19}
$^3K_8$-$^5I_8$	0.02	0.03	0.15	3.01×10^{-21}	7.74×10^{-21}
$^5F_3$-$^5I_8$	0.00	0.00	0.34	7.71×10^{-21}	9.01×10^{-21}
$^5F_4$-$^5I_8$	0.00	0.23	0.93	6.20×10^{-20}	4.54×10^{-20}
$^5F_5$-$^5I_8$	0.00	0.42	0.56	5.88×10^{-20}	5.22×10^{-20}
$^5I_7$-$^5I_8$	0.02	0.13	1.52	4.04×10^{-20}	5.23×10^{-20}

$$\times \int Abs(\lambda)\mathrm{d}\lambda \tag{1}$$

where J is the total angular momentum, n_s is the refractive index of the microsphere, N_0 is the particle concentration, L is the thickness of the bulk glass, and λ is the wavelength.

The phenomenological intensity parameters, Ω_2, Ω_4, and Ω_6, were obtained by fitting the above results. The corresponding theoretical value (S_{theory}) could also be calculated as follows:

$$S_{\text{Theory}}\left(J \to J'\right) = \sum_{t=2,4,6} \Omega_t \left|\left\langle 4f^n\left[S,L\right]J \left\| \mathrm{U}^{(t)} \right\| 4f^n\left[S',L'\right]J' \right\rangle\right|^2 \tag{2}$$

where S and L are the total spin and orbital angular momenta, and $\mathrm{U}^{(t)}$ is the reduced matrix element of the rare-earth material. In order to determine the correctness of the fitting of the absorption spectrum, it was necessary to calculate the relative error from:

$$\delta\text{error} = \sqrt{\sum \left(S_{\text{exp}} - S_{\text{theory}}\right)^2/(M-3)} \Big/ \sqrt{\sum S_{\text{exp}}^2/M} \tag{3}$$

where M is the number of absorption peaks.

The calculation results are summarized in Table II, which shows the transition from the higher energy level to the ground level, the corresponding reduction matrix (U(2), U(4) and U(6)), and the experimental and theoretical linewidth strengths (S_{exp} and S_{theory}). The Ω_2, Ω_4, and Ω_6 values obtained were 3.33×10^{20} cm^2, 8.80×10^{20} cm^2 and 2.60×10^{20} cm^2, respectively. The relative error, δ, calculated from the experiment is approximately 12% and is mainly due to the high background noise in Fig. 1(a) and the sensitivity of the detector.

TABLE III
EMISSION TRANSITION PROBABILITY OF CORRESPONDING ENERGY LEVEL TRANSITION

Transition	Wavelength (μm)	A_{ed} (s^{-1})	A_{md} (s^{-1})	β	τ (s)
$^5I_6$-$^5I_8$	2.86	65.5	239	0.132	1.12×10^{-2}
$^5I_6$-$^5I_8$	1.17	590	0.568	0.868	1.69×10^{-3}
$^5I_7$-$^5I_8$	1.98	245	1.52	1.00	3.45×10^{-3}

In addition, considering the energy level transitions involved in this microsphere laser test, the electric dipole transition probability, A_{ed}, the magnetic dipole transition probability, A_{md}, the total transition probability, the emission lifetime, τ, and the fluorescence branch ratio, β, of the $^5I_6$, $^5I_7$ and $^5I_8$ energy levels of Ho^{3+} were calculated and the results for the respective transitions are shown in Table III.

Next, we consider the solution of the internal dynamic characteristics in a microsphere laser. Initially, the mode of the signal light propagating in the microsphere can be determined by analyzing the red line in Fig. 2(b), from which it can be concluded that the TE mode number is $l = 93$, $n = 3$ when the wavelength is 2.08 μm [48] using in-house developed code. It is assumed that the tapered fiber and the microsphere have good phase-matching when determining the mode of the signal light propagation in the microsphere. As can be seen from Fig. 3, the blue lines represent the relationship between the effective refractive index and the radius of the microsphere, the effective index decreases significantly as the radial order, n, increases from the 1st order to the 7th order [49]. The black line in Fig. 3 represents the relationship between the effective refractive index and the radius of the tapered fiber. Rare-earth doped compound glasses generally have a higher refractive index compared to silica. Therefore, in order to achieve better phase-matching between the tapered fiber and the microsphere, the size of the microsphere was reduced as much as possible for the experiments. It can be seen from Fig. 3, that there is a green intersection point between the red dotted line and the blue line, which corresponds to the radius of the microsphere used in the experiment. Thus, the TE mode number of the pump light in the microsphere was determined to be $l = 158$, $n = 7$.

According to the electric field distribution in the microsphere [50], the ratio of the optical field energy transmitted in the gain medium to the total optical field energy can be obtained, so the effective mode overlap of the pumped light and the signal light can be expressed as follows:

$$\Gamma = \frac{P_{\text{inside}}}{P_{\text{total}}} = \frac{\int_0^{\pi}\int_0^{r} I(r)r\mathrm{d}r\mathrm{d}\theta}{\int_0^{\pi}\int_0^{\infty} I(r)r\mathrm{d}r\mathrm{d}\theta} \tag{4}$$

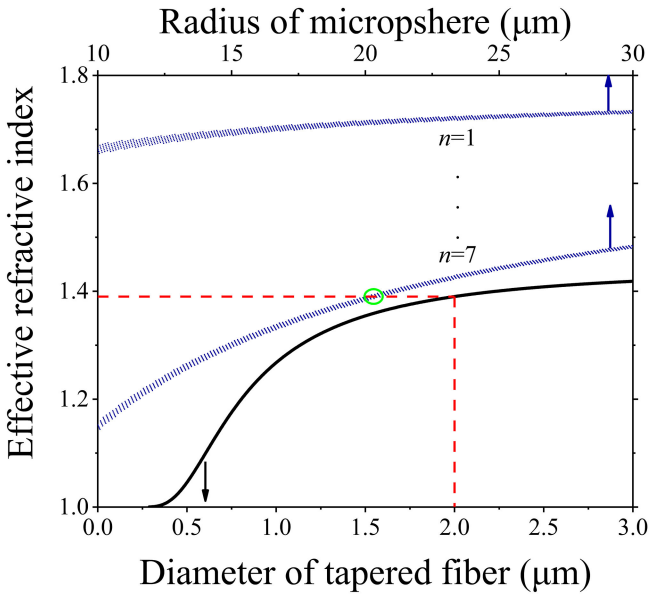

Fig. 3. The blue dots represent the effective refractive of different modes ($n = 1$ and 7) as a function of the radius of the microsphere and the black line as a function of tapered fiber.

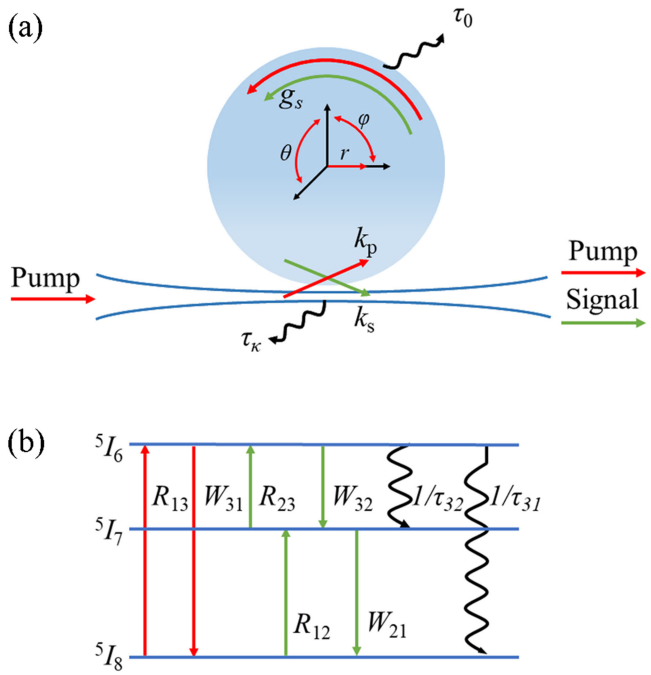

Fig. 4. (a) Schematic coupling of the tapered fiber and microsphere, where r, φ, and θ are the radial, azimuthal, and polar directions in the microsphere. (b) Simplified energy level diagram for Ho^{3+} ions.

where P_{inside} and P_{total} are the power inside and total power of the microsphere, I is the intensity of the electric field of the light propagating in the microsphere, r and θ are the radial and polar directions in the microsphere.

Figure 4(a) is a schematic diagram of the tapered fiber and microsphere system, in which the wavelength of the pump light and the signal light are 1.15 μm and 2.08 μm, respectively, and g_s is the gain of the light signal in the microsphere generated by population inversion of the Ho^{3+} ions, defined as:

$$g_s = \Gamma_s \cdot (\sigma_{12} N_2 - \sigma_{21} N_1) \tag{5}$$

where N_1, N_2 and N_3 are the population concentrations of the $^5I_6$, $^5I_7$, and $^5I_8$ energy levels respectively, and σ_{12} (σ_{21}) is the absorption (emission) cross-section of the signal light. τ_0 is the material loss in the microsphere, mainly determined from the Q-factor [1], τ_k is the coupling loss, and k_p (k_s) is the coupling coefficient of the pump (signal) light [50], where $k_p = 28.23$ ($l = 158$, $n = 7$) and $k_s = 0.23$ ($l = 93$, $n = 3$) in corresponding mode. Figure 4(b) represents the energy level diagram of the Ho^{3+} ions, where the R_{ij}, W_{ij} and $1/\tau_{ij}$ represent the stimulated absorption and emission probabilities, and the decay lifetime values from the i to j energy level, respectively.

Finally, considering the population in the $^5I_6$, $^5I_7$, and $^5I_8$ energy levels of Ho^{3+} and the light-matter interactions in the microsphere [44], the ordinary differential equations (ODE) that govern the light emission process can be formulated as follows:

$$\frac{dN_1}{dt} = -(W_{12} + R_{13}) \cdot N_1 + (W_{21} + A_{21}) \cdot N_2 + A_{31} N_3 \tag{6}$$

$$\frac{dN_2}{dt} = W_{12} N_1 - (W_{21} + A_{21}) \cdot N_2 + (W_{32} + A_{32}) \cdot N_3 \tag{7}$$

$$\frac{dN_3}{dt} = R_{13} N_1 + W_{23} N_2 - (A_{31} + A_{32} + W_{32}) \cdot N_3 \tag{8}$$

$$\frac{dP_{l2}(t)}{dt} = c \cdot (g_s - \alpha_s - \kappa_s) \cdot P_{l2}(t) - 2h\nu_s \Delta\nu_s \Gamma_{12} \sigma_{21} N_2 \tag{9}$$

$$N_{tol} = N_1 + N_2 + N_3 \tag{10}$$

$$R_{13} = \Gamma_p / (A_P h\nu_p) \cdot P(t) \tag{11}$$

$$W_{12} = \Gamma_s / (A_s h\nu_s) \cdot P_{l2}(t) \tag{12}$$

where P_{l2} and P are the laser power and the pump power, N_{tol} is the total population density, A_p and A_s are the effective mode areas of the pump light and signal light, A_{31}, A_{32} and A_{21} are spontaneous emission probabilities between energy levels, $\Delta\nu_s$ is the linewidth of the signal light, h is Planck's constant, and ν_p and ν_s are the frequency of the pump source and the output laser. In order to simplify the simultaneous ODEs in the above calculation, an average pump power, P(t), is proposed, with:

$$\int_0^L P_p e^{(g_p - \alpha_p) \cdot x} dx = P(t) \cdot L \tag{13}$$

$$P(t) = P_p \cdot (e^{(g_p - \alpha_p) \cdot L} - 1) / (L \cdot (g_p - \alpha_p)) \tag{14}$$

where L is the circumference of the microsphere, P_p is the power coupled into the microsphere, and g_p (α_p) represents gains (losses) in the microsphere.

The dynamic characteristics of the microsphere laser can thus be obtained by combining A_{ed}, A_{md}, β and τ, calculated using the previously stated J-O theory. Figure 5(a) shows the relationship between the population of each energy level and time, and

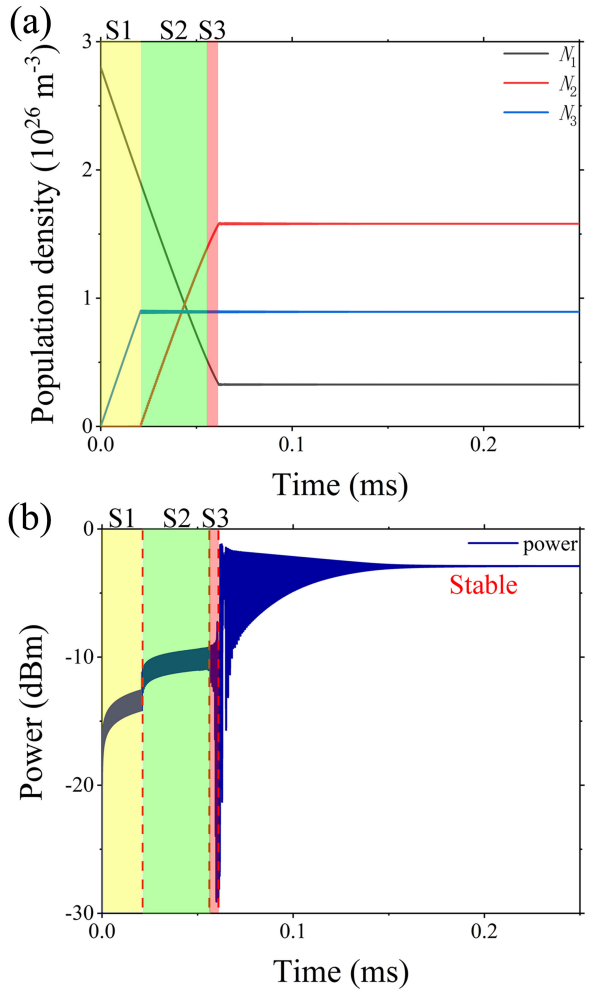

Fig. 5. (a) Time evolution of the population density in the $^5I_6$, $^5I_7$, and $^5I_8$ energy levels and (b) output laser power over time. The yellow, green, and red areas represent the S1, S2, and S3 stages, respectively.

Fig. 5(b) shows the power of the output laser at a wavelength of 2 μm on the same time axis. In the first stage, S1, for a time interval from 0 to 0.02 ms (see Fig. 5(b)), the population in the ground state is mainly pumped to the $^5I_6$ level. In the second stage, S2, for a time interval from 0.02 to 0.056 ms, the ground state population continues to decrease, and the population in the $^5I_7$ level begins to exceed the value in the $^5I_6$ level, thereby increasing the intensity of the signal light. In the third stage, S3, when the time reaches 0.061 ms, relaxation oscillation happens due to the largest population difference between the $^5I_6$ and $^5I_7$ energy levels. In these circumstances, the power of the signal light in the microsphere becomes stable, and finally the power of the stable output laser is -2.9 dBm (1.25 μW) when the pump power is set to 550 μW.

VI. Conclusion

In conclusion, we have fabricated a 2 μm low-threshold microsphere laser based on Ho^{3+} doped tellurite glass and we have theoretically described its operation from a consideration of the dynamic energy transitions within the microsphere that govern the output light signal emission at 2 μm. In the experiment, the bulk glasses were characterized in terms of their absorption and emission spectra, and fluorescence lifetime. In addition, the microsphere was pumped using a single-mode fiber laser at 1150 nm, yielding the 2 μm laser output with a low-threshold of 342 μW. In the theoretical simulations, the emission probability, fluorescence branch ratio, and energy level lifetime were calculated using J-O theory. Combined with the population rate equations for the rare-earth ions and the light-matter interaction in the microsphere, the dynamic characteristics of the microsphere laser were successfully simulated, it is helpful for any future work on compound glass microsphere lasers and demonstrates that the host material should not be overlooked in theoretical investigation. The research reported in this article has major potential impact in many applications, including microcavity laser sources operating in the mid-infrared range, integrated active photonic devices, and laser sensing using microcavity resonators based on compound glass.

References

[1] A. Chiasera *et al.*, "Spherical whispering-gallery-mode microresonators," *Laser Photon. Rev.*, vol. 4, no. 3, pp. 457–482, 2010.
[2] L. He, Ş. K. Özdemir, and L. Yang, "Whispering gallery microcavity lasers," *Laser Photon. Rev.*, vol. 7, no. 1, pp. 60–82, 2013.
[3] M. L. Gorodetsky, A. A. Savchenkov, and V. S. Ilchenko, "Ultimate Q of optical microsphere resonators," *Opt. Lett.*, vol. 21, no. 7, pp. 453–455, 1996.
[4] J. U. Nöckel, "Optical feedback and the coupling problem in semiconductor microdisk lasers," *Physica Status Solidi A.*, vol. 188, no. 3, pp. 921–928, 2001.
[5] S. M. Spillane, T. J. Kippenberg, and K. J. Vahala, "Ultralow-threshold Raman laser using a spherical dielectric microcavity," *Nature*, vol. 415, no. 6872, pp. 621–623, 2002.
[6] I. S. Grudinin and L. Maleki, "Ultralow-threshold Raman lasing with CaF_2 resonators," *Opt. Lett.*, vol. 32, no. 2, pp. 166–168, 2007.
[7] Q. Q. Xiong *et al.*, "Synthesis of hierarchical hollow-structured single-crystalline magnetite (Fe_3O_4) microspheres: The highly powerful storage versus lithium as an anode for lithium ion batteries," *J. Physical Chem. C*, vol. 116, no. 10, pp. 6495–6502, 2012.
[8] D. Farnesi, A. Barucci, G. C. Righini, S. Berneschi, S. Soria, and G. Nunzi Conti, "Optical frequency conversion in silica-whispering-gallery-mode microspherical resonators," *Physical Rev. Lett.*, vol. 112, no. 9, 2014, Art. no. 093901.
[9] C.-H. Dong, Z. Shen, C.-L. Zou, Y.-L. Zhang, W. Fu, and G.-C. Guo, "Brillouin-scattering-induced transparency and non-reciprocal light storage," *Nature Commun.*, vol. 6, 2015, Art. no. 6193.
[10] J. Kim, M. C. Kuzyk, K. Han, H. Wang, and G. Bahl, "Non-reciprocal Brillouin scattering induced transparency," *Nature Phys.*, vol. 11, pp. 275–280, 2015.
[11] X. Jin, J. Wang, M. Wang, Y. Dong, F. Li, and K. Wang, "Dispersion engineering of a microsphere via multi-layer coating," *Appl. Opt.*, vol. 56, no. 28, pp. 8023–8028, 2017.
[12] M. Cai, O. Painter, K. J. Vahala, and P. C. Sercel, "Fiber-coupled microsphere laser," *Opt. Lett.*, vol. 25, no. 19, pp. 1430–1432, 2000.
[13] F. Lissillour, D. Messager, G. Stéphan, and P. Féron, "Whispering-gallery-mode laser at 1.56 μm excited by a fiber taper," *Opt. Lett.*, vol. 26, no. 14, pp. 1051–1053, 2001.
[14] K. Totsuka and M. Tomita, "Optical microsphere amplification system," *Opt. Lett.*, vol. 32, no. 21, pp. 3197–3199, 2007.
[15] Y. Wu, J. M. Ward, and S. Nic Chormaic, "Ultralow threshold green lasing and optical bistability in ZBNA (ZrF_4–BaF_2–NaF–AlF_3) microspheres," *J. Appl. Phys.*, vol. 107, no. 3, 2010, Art. no. 033103.
[16] V. H. Pham *et al.*, "Control of whispering-gallery-mode spectrum from erbium-doped silica microsphere lasers," *J. Opt. Soc. Amer. B*, vol. 30, no. 6, pp. 1586–1589, 2013.
[17] Y. Yang *et al.*, "Tunable erbium-doped microbubble laser fabricated by sol-gel coating," *Opt. Exp.*, vol. 25, no. 2, pp. 1308–1313, 2017.

[18] X. Wang, Y. Yu, S. Wang, J. M. Ward, S. Nic Chormaic, and P. Wang, "Single mode green lasing and multicolor luminescent emission from an Er^{3+}-Yb^{3+} co-doped compound fluorosilicate glass microsphere resonator," *OSA Continuum*, vol. 1, no. 1, pp. 261–273, 2018.

[19] T. Ouyang *et al.*, "Microlaser output from rare-earth ion-doped nanocrystal-in-glass microcavities," *Adv. Opt. Mater.*, vol. 7, no. 21, 2019, Art. no. 1900197.

[20] L. Brillouin, "Diffusion de la lumière et des rayons X par un corps transparent homogène," *Ann. Phys.*, vol. 9, no. 17, pp. 88–122, 1922.

[21] G. R. Elliott, G. S. Murugan, J. S. Wilkinson, M. N. Zervas, and D. W. Hewak, "Chalcogenide glass microsphere laser," *Opt. Exp.*, vol. 18, no. 25, pp. 26720–26727, 2010.

[22] G. S. Murugan, M. N. Zervas, Y. Panitchob, and J. S. Wilkinson, "Integrated Nd-doped borosilicate glass microsphere laser," *Opt. Lett.*, vol. 36, no. 1, pp. 73–75, 2011.

[23] P. Wang *et al.*, "Lead silicate glass microsphere resonators with absorption-limited Q," *Appl. Phys. Lett.*, vol. 98, no. 18, 2011, Art. no. 181105.

[24] Q. Liu, B. F. Johnston, S. Gross, M. J. Withford, and M. J. Steel, "A parametric study of laser induced-effects in terbium-doped borosilicate glasses: Prospects for compact magneto-optic devices," *Opt. Mater. Exp.*, vol. 3, no. 12, pp. 2096–2111, 2013.

[25] T. Wu, Y. Huang, J. Huang, Y. Huang, P. Zhang, and J. Ma, "Laser oscillation of Yb^{3+}:Er^{3+} co-doped phosphosilicate microsphere [Invited]," *Appl. Opt.*, vol. 53, no. 21, pp. 4747–4751, 2014.

[26] Z. Fang *et al.*, "Bismuth-doped glass microsphere lasers," *Photon. Res.*, vol. 5, no. 6, pp. 740–744, 2017.

[27] J. Yu, E. Lewis, G. Farrell, and P. Wang, "Compound glass microsphere resonator devices," *Micromachines*, vol. 9, no. 7, 2018, Art. no. 356.

[28] L. Mescia, P. Bia, M. De Sario, A. Di Tommaso, and F. Prudenzano, "Design of mid-infrared amplifiers based on fiber taper coupling to erbium-doped microspherical resonator," *Opt. Exp.*, vol. 20, no. 7, pp. 7616–7629, 2012.

[29] L. Mescia, P. Bia, O. Losito, and F. Prudenzano, "Design of mid-IR Er^{3+} -doped microsphere laser," *IEEE Photon. J.*, vol. 5, no. 4, Dec. 2013, Art. no. 1501308.

[30] G. Palma *et al.*, "Design of praseodymium-doped chalcogenide micro-disk emitting at 4.7 μm," *Opt. Exp.*, vol. 25, no. 6, pp. 7014–7030, 2017.

[31] S. B. Rai, A. K. Singh, and S. K. Singh, "Spectroscopic properties of Ho^{3+} ions doped in tellurite glass," *Spectrochimica Acta Part A: Mol. Biomolecular Spectros.*, vol. 59, no. 14, pp. 3221–3226, 2003.

[32] C. A. Evans, Z. Ikonić, B. Richards, P. Harrison, and A. Jha, "Numerical rate equation modeling of a $\sim$2.1 μm-Tm^{3+}/Ho^{3+} Co-doped tellurite fiber laser," *J. Lightw. Technol.*, vol. 27, no. 19, pp. 4280–4288, Oct. 2009.

[33] C. M. Dodson and R. Zia, "Magnetic dipole and electric quadrupole transitions in the trivalent lanthanide series: Calculated emission rates and oscillator strengths," *Physical Rev. B*, vol. 86, no. 12, 2012, Art. no. 125102.

[34] S. Tanabe, "Rare-earth-doped glasses for fiber amplifiers in broadband telecommunication," *Comptes Rendus Chimie*, vol. 5, no. 12, pp. 815–824, 2002.

[35] V. V. R. K. Kumar, A. K. George, J. C. Knight, and P. S. J. Russell, "Tellurite photonic crystal fiber," *Opt. Exp.*, vol. 11, no. 20, pp. 2641–2645, 2003.

[36] X. Feng *et al.*, "Towards water-free tellurite glass fiber for 2–5 μm nonlinear applications," *Fibers*, vol. 1, no. 3, pp. 70–81, 2013.

[37] J. Zhang *et al.*, "2.8 μm emission and OH quenching analysis in Ho^{3+} doped fluorotellurite-germanate glasses sensitized by Yb^{3+} and Er^{3+}," *Sci. Rep.*, vol. 7, no. 1, 2017, Art. no. 16794.

[38] Y. Dong, K. Wang, and X. Jin, "Packaged microsphere-taper coupling system with a high Q factor," *Appl. Opt.*, vol. 54, no. 2, pp. 277–284, 2015.

[39] M. Sumetsky, Y. Dulashko, and R. S. Windeler, "Super free spectral range tunable optical microbubble resonator," *Opt. Lett.*, vol. 35, no. 11, pp. 1866–1868, 2010.

[40] H. Y. Zhao *et al.*, "A Tm^{3+}-doped ZrF_4-BaF_2-YF_3-AlF_3 glass microsphere laser in the 2.0 μm wavelength region," *J. Lumin.*, vol. 212, pp. 207–211, 2019.

[41] L. Peng, Y. Huang, Y. Duan, S. Zhuang, T. Liao, and C. Xu, "2 μm laser oscillation of Ho^{3+}:Tm^{3+}-codoped silica microspheres," *Appl. Opt.*, vol. 56, no. 26, pp. 7469–7473, 2017.

[42] A. Li *et al.*, "Effect of Tm^{3+} concentration on the emission wavelength shift in Tm^{3+}-doped silica microsphere lasers," *Opt. Lett.*, vol. 43, no. 18, pp. 4325–4328, 2018.

[43] A. Li *et al.*, "An Yb^{3+}-Ho^{3+} codoped glass microsphere laser in the 2 μm wavelength regions," *IEEE Photon. Technol. Lett.*, vol. 30, no. 17, pp. 1543–1546, Sep. 2018.

[44] Z. Yang *et al.*, "Fabrication and characterization of Tm^{3+}-Ho^{3+} co-doped tellurite glass microsphere lasers operating at $\sim$2.1 μm," *Opt. Mater.*, vol. 72, pp. 524–528, 2017.

[45] J. Wu, S. Jiang, T. Qua, M. Kuwata-Gonokami, and N. Peyghambarian, "2 μm lasing from highly thulium doped tellurite glass microsphere," *Appl. Phys. Lett.*, vol. 87, no. 21, 2005, Art. no. 211118.

[46] B. R. Judd, "Optical absorption intensities of rare-earth ions," *Physical Rev.*, vol. 127, no. 3, pp. 750–761, 1962.

[47] G. S. Ofelt, "Intensities of crystal spectra of rare-earth ions," *J. Chem. Phys.*, vol. 37, no. 3, pp. 511–520, 1962.

[48] S. Schiller, "Asymptotic expansion of morphological resonance frequencies in Mie scattering," *Appl. Opt.*, vol. 32, no. 12, pp. 2181–2185, 1993.

[49] V. S. Ilchenko, X. S. Yao, and L. Maleki, "Pigtailing the high-Q microsphere cavity: a simple fiber coupler for optical whispering-gallery modes," *Opt. Lett.*, vol. 24, no. 11, pp. 723–725, 1999.

[50] B. E. Little, J. Laine, and H. A. Haus, "Analytic theory of coupling from tapered fibers and half-blocks into microsphere resonators," *J. Lightw. Technol.*, vol. 17, no. 4, pp. 704–715, Apr. 1999.